Available online at www.sciencedirect.com
ScienceDirect
Journal of Magnetic Resonance 189 (2007) 182–189
JMR Journal of Magnetic Resonance
www.elsevier.com/locate/jmr

Low-E probe for ^{19}F–^{1}H NMR of dilute biological solids

Peter L. Gor'kov [a,*], Raiker Witter [b], Eduard Y. Chekmenev [a,c], Farhod Nozirov [a], Riqiang Fu [a,d], William W. Brey [a]

[a] National High Magnetic Field Laboratory, 1800 East Paul Dirac Drive, Tallahassee, FL 32310, USA
[b] Forschungszentrum Karlsruhe, IBG, POB 3640, 76021 Karlsruhe, Germany
[c] Huntington Medical Research Institutes and California Institute of Technology, Pasadena, CA 91105, USA
[d] Department of Chemistry, Florida State University, Tallahassee, FL 32306, USA

Received 18 July 2007; revised 5 September 2007
Available online 18 September 2007

Abstract

Sample heating induced by radio frequency (RF) irradiation presents a significant challenge to solid state NMR experiments in proteins and other biological systems, causing the sample to dehydrate which may result in distorted spectra and a damaged sample. In this work we describe a large volume, low-E ^{19}F–^{1}H solid state NMR probe, which we developed for the 2D ^{19}F CPMG studies of dilute membrane proteins in a static and electrically lossy environment at 600 MHz field. In ^{19}FCPMG and related multi-pulse ^{19}F–^{1}H experiments the sample is heated by the conservative electric fields E produced in the sample coil at both ^{19}F and ^{1}H frequencies. Instead of using a traditional sample solenoid, our low-E ^{19}F–^{1}H probe utilizes two orthogonal loop-gap resonators in order to minimize the conservative electric fields responsible for sample heating. Absence of the wavelength effects in loop-gap resonators results in homogeneous RF fields and enables the study of large sample volumes, an important feature for the dilute protein preparations. The orthogonal resonators also provide intrinsic isolation between the ^{19}F and ^{1}H channels, which is another major challenge for the ^{19}F–^{1}H circuits where Larmor frequencies are only 6% apart. We detail steps to reduce ^{19}F background signals from the probe, which included careful choice of capacitor lubricants and manufacture of custom non-fluorinated coaxial cables. Application of the probe for two-dimensional ^{19}F CPMG spectroscopy in oriented lipid membranes is demonstrated with Flufenamic acid (FFA), a non-steroidal anti-inflammatory drug.

Keywords: RF sample heating; Fluorine NMR; Membrane proteins; Dielectric loss; Loop-gap resonator; Flat coil probe; Solid state NMR probe; Low-E; LGR; Alderman-Grant

1. Introduction

Solid state ^{19}F NMR has emerged as a versatile tool for investigating the structure and dynamics of biological systems [1–3]. Fluorine's advantages as a molecular probe include the absence of a natural biological background, an exceptional NMR sensitivity, a spin 1/2, a strong dipolar coupling, and a chemical shift range of more than a hundred ppm [4–7]. A fluorine atom can be substituted for a hydrogen atom or OH group in amino acids with little effect on structure and dynamics. A number of ^{19}F-labeled amino acids are now routinely incorporated in peptides and proteins: 4F-Phg, 4-CF_3-Phg, 3F-Ala, 5F-Trp, 6F-Trp, 4F-Phe, 3F-Phe, 3F-Tyr, δF-Leu, δF3-Leu, γF-Val, and γF_3-Val [3].

Unfortunately, the strong radio-frequency fields needed for solid state NMR techniques can readily heat the protein samples, resulting in distorted spectra and eventual dehydration of the sample [8–10]. High magnetic field, with its correspondingly high ^{1}H Larmor frequency, greatly exacerbates this problem [11,12]. A number of recent articles address ^{1}H decoupler heating in biological solids by using low-inductance RF coils that subject the sample to lower conservative electric fields in comparison with conventional

* Corresponding author. Fax: +1 850 644 1366.
E-mail address: pgorkov@magnet.fsu.edu (P.L. Gor'kov).

1090-7807/$ - see front matter © 2007 Elsevier Inc. All rights reserved.
doi:10.1016/j.jmr.2007.09.008

solenoids [13–16]. Since the Larmor frequency of ^{19}F is only 6% apart from that of ^{1}H, ^{19}F irradiation during Carr–Purcell–Meiboom–Gill (CPMG) [17,18] or related multi-pulse experiments also contributes to sample heating. Isolation between the detection and decoupling channels is another important issue for effective ^{19}F–^{1}H probes. With the ^{19}F detection frequency lying so close to the ^{1}H decoupling frequency, it is difficult to achieve the >80 dB isolation from decoupler noise required for dilute samples. In order to obtain this level of isolation, a double-tuned sample coil with separate inputs for ^{19}F and ^{1}H channels requires elaborate filtering implemented both inside and outside the probe. Another well known approach utilizes two overcoupled resonators with a single port for both ^{19}F and ^{1}H channels, and then employs an external splitter and filters [19–23]. Although this approach may require iterative tuning, it has been used in commercial solid state probes equipped with solenoidal sample coils. However, our attempts to tune and match a low-inductance sample coil (~10 nH or less) with such a circuit for use with heat sensitive biological solids resulted in a probe with very unstable and unwieldy tuning.

In this article, we describe a large volume 600 MHz ^{19}F–^{1}H flat coil probe designed for studies of heat sensitive and dilute samples of membrane proteins oriented in hydrated lipid bilayers. Our design employs orthogonal low-E sample resonators [15] for both the ^{19}F and ^{1}H channels, with the aim to reduce sample heating from irradiation at both frequencies. The resonators are nested, with the ^{19}F resonator placed on the inside to provide the greatest sensitivity. Separate single resonance matching networks drive each resonator, eliminating complex traps and filters from the probehead. The low mutual inductance of this orthogonal low-E approach provides $\geqslant$ 23 dB of isolation between the two frequencies within the probehead, without outside filters. The independent tuning networks and low mutual inductance between the resonators remove the need for iterative tuning typical of single-port designs. We also describe special steps taken for the reduction of ^{19}F background and demonstrate an application of the probe for two-dimensional ^{19}F CPMG spectroscopy in oriented lipid membranes.

2. Methods

2.1. Nested low-E coil assembly

The ^{19}F–^{1}H flat sample probe presented here utilizes two orthogonal resonators nested together as shown in Fig. 1. The outer coil is a rectangular loop-gap resonator (LGR) that produces a ^{1}H magnetic field, normally used for decoupling, along the y-axis. It is identical in design and dimension to the ^{1}H resonator in a previously described ^{15}N–^{1}H probe for PISEMA experiments [15]. The inner, ^{19}F observe resonator is a variation of an Alderman-Grant coil [24] with internal dimensions of $8.1 \times 5.8 \times 10$ mm closely matching the size and shape of the rectangular sample cell for maximum sensitivity. It is formed from 0.38 mm copper foil, which was chosen to be strong enough to maintain its shape without additional reinforcement. The bottom and top halves of the ^{19}F resonator are joined at the corners by four 100B series non-magnetic chip capacitors from ATC (American Technical Ceramics, Huntington, Station, NY) each measuring 15.3 pF. The resulting Alderman-Grant coil is held in place inside the larger ^{1}H loop-gap resonator by two tightly fitting low-loss dielectric plates (Rexolite™, Boedeker Plastics, Shiner, TX). The coils are arranged to allow unobstructed insertion of a sample cell along the x-axis, through the rectangular sample-shaped openings in the ^{1}H LGR.

The ^{19}F resonator must be further modified from the traditional Alderman-Grant configuration to perform well within the ^{1}H coil. The values of the chip capacitors in the ^{19}F resonator are large enough to allow substantial ^{1}H eddy currents around the two openings perpendicular to the y-axis, causing a drastic loss of efficiency in the decoupling channel. To remedy both of these problems, a slit has been placed across the top plane of the ^{19}F resonator as shown in Figs. 1 and 2, interrupting the path for ^{1}H eddy currents. A traditional Alderman-Grant coil [24] without guard rings has 3 resonant modes, two of which provide homogeneous magnetic field in the x- and y-direction. We are only interested in the mode that produces homogeneous ^{19}F B_1 along the x-axis—orthogonally to the ^{1}H B_1. The slot reduces the number of resonant modes in the ^{19}F

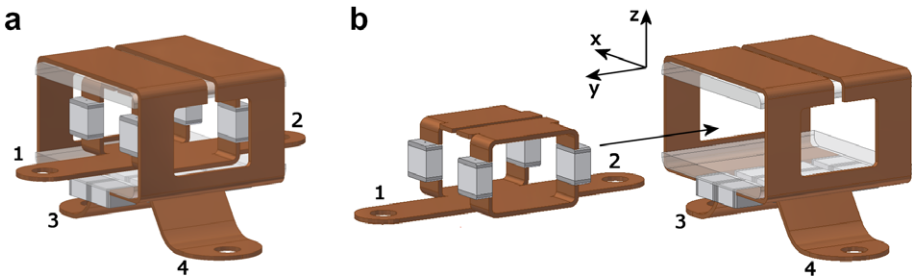

Fig. 1. Design of the nested ^{19}F–^{1}H low-E flat coil (a) and its mechanical assembly (b). A double-gap ^{19}F resonator is inserted into a ^{1}H loop-gap resonator, where it is supported by two dielectric spacers. The resonators are oriented to produce RF fields in orthogonal directions. The homogeneous mode of the ^{19}F coil produces a B_1 field in x-direction, whereas the ^{1}H LGR produces a B_1 field in the y-direction. The nested low-E assembly is attached to an RF circuit below with 4 screws using holes 1, 2 (^{19}F) and 3, 4 (^{1}H).

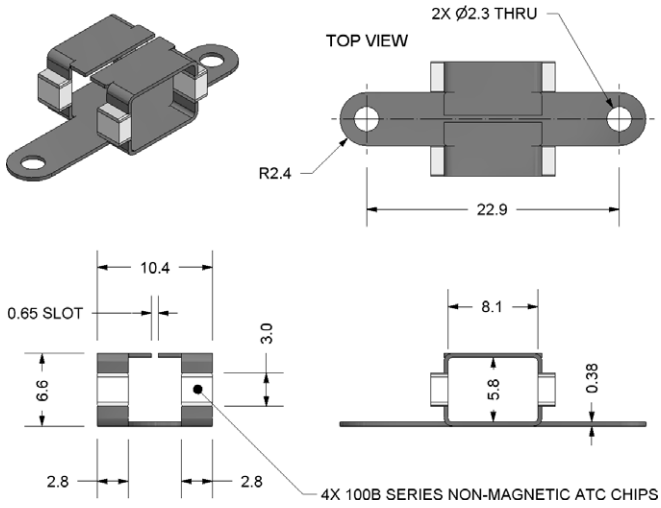

Fig. 2. Physical dimensions of the inner ^{19}F flat sample resonator, in millimeters.

coil from 3 to 2. Of these remaining 2 modes, $f_0 = 581$ MHz and $f_1 = 724$ MHz, only f_0 generates a homogeneous magnetic field along the x-axis. The other mode f_1, consisting of counter-rotating currents, generates zero field in the middle of the coil. The resonances f_0 and f_1 above were measured on the bench with the ^{19}F resonator removed from the matching network and the ^{1}H resonator.

When connecting the ^{19}F resonator to its matching network, it is important not to reconnect the resonator across the top slot and re-create a path for ^{1}H eddy currents. To avoid this, the ^{19}F resonator is fed across its conductive bottom plane, which is modified accordingly to incorporate the lead extensions (Figs. 1 and 2). Another possibility is to feed ^{19}F resonator across any single chip capacitor at some cost to the spatial homogeneity of the RF field. The exact physical dimensions of the inner ^{19}F resonator are shown in Fig. 2. Once the ^{19}F resonator has been inserted into the ^{1}H resonator, the whole assembly is connected to the probe's ^{19}F and ^{1}H matching networks by means of four non-magnetic brass screws, using holes 1, 2, and 3, 4, respectively (Figs. 1 and 3).

2.2. Probe RF circuit

The two orthogonal resonators in this low-E ^{19}F–^{1}H flat coil probe are driven by independent single-resonance balanced circuits similar to those described in our article on the ^{15}N–^{1}H PISEMA probe [15]. The chip capacitors within each resonator were chosen to bring its standalone resonance frequency f_0 just slightly above the respective Larmor frequency f. This allows for a small but sufficient tuning range while maximizing the current that flows around the sample and hence the B_1. The circuit components outside the resonators are relegated to line matching and to fine sample-dependent tuning adjustments, which are inherently small due to the reduction of electric field achieved in low-E coils. We used $f_0 = 581$ MHz for the ^{19}F ($f = 564$ MHz) and $f_0 = 631$ MHz for the ^{1}H ($f = 600$ MHz) resonators.

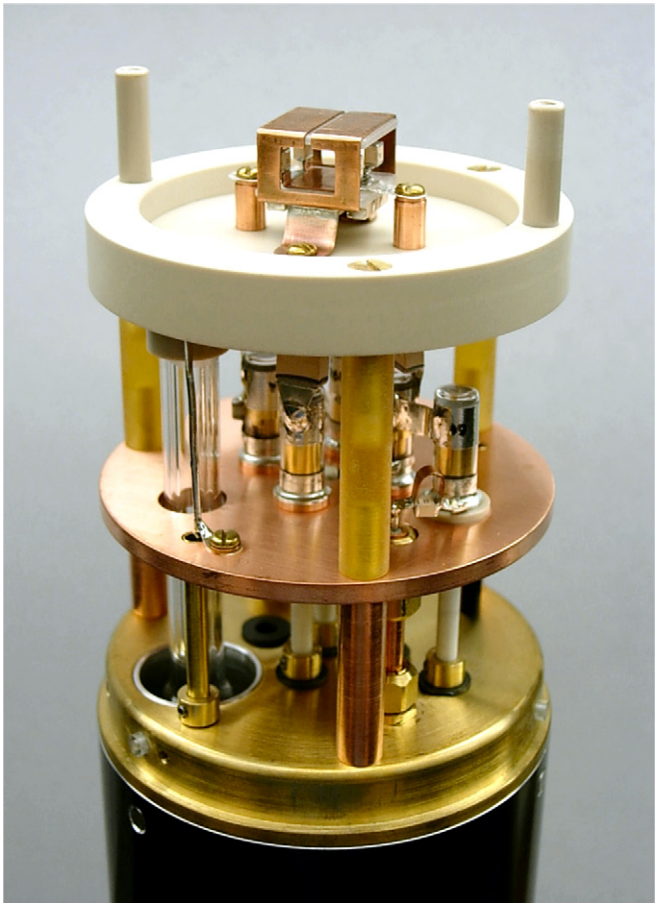

Fig. 3. Photograph of the probehead.

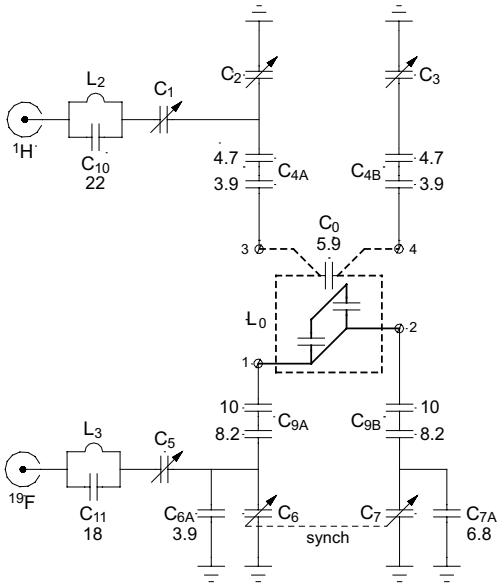

Fig. 4. RF circuit of the 600 MHz low-E ^{19}F–^{1}H flat coil probe. The nested low-E coil assembly consists of a rectangular ^{19}F double-gap resonator (thick solid outline) inside a ^{1}H loop-gap resonator L_0–C_0 (thick dash). The two resonators are oriented to produce B_1 fields in orthogonal directions. See the text and Figs. 1 and 2 for more details on the inner ^{19}F resonator.

Figs. 3 and 4 show the layout and RF circuit of our ^{19}F–^{1}H probe. The matching network for the ^{1}H loop-gap resonator (L_0–C_0) and its operation have been described previously [15]. Matching and tuning of the ^{1}H channel is accomplished by variable capacitors C_1 and C_3, respectively. C_2 is a symmetry capacitor whose purpose is to equalize voltage amplitudes at the sides of the gap capacitor C_0. C_2 reduces the maximum electric field at the terminals of C_0 and thereby reduces the possibility of arcing to the ^{19}F resonator or other conductors at lower potential. A properly balanced resonator can therefore sustain a higher B_1 field without arcing during long decoupling pulses. Voltronics 11 series chip capacitors C_{4A} and C_{4B} serve as voltage dividers that safeguard the trimmer capacitors C_2 and C_3. In the previously described PISEMA probe we used high voltage trimmer capacitors made with PTFE dielectric. However, the presence of these capacitors in either of this probe's two channels leads to a strong ^{19}F background signal. Therefore our choice of trimmer capacitors was limited to models made with quartz or glass dielectric, which in general are rated to withstand less voltage. The variable trimmer capacitors used for this probe are from the relatively low-voltage NMQM quartz series manufactured by Voltronics Corporation (Denville, NJ). Specifically, they are the NMQM3G and NMQM6GE non-magnetic quartz models, only these were modified to eliminate the strong ^{19}F background from commercial lubricants used by Voltronics in its standard manufacturing process (see Section 2.3 below).

The RF circuit driving the ^{19}F resonator is very similar to that employed in the ^{1}H channel. Fixed capacitors C_{9A} and C_{9B} (11 series Voltronics chips) reduce the voltage experienced by the quartz trimmers located underneath. Matching the ^{19}F resonance to 50 Ω is done with variable capacitor C_5 (NMQM3G). Tuning capacitors C_6 and C_7 (NMQM6GE) have their extended shafts connected by a 3-gear mechanism to a single tuning rod that changes positions of both pistons at the same rate, automatically readjusting the circuit balance as the ^{19}F channel is tuned. We find that maintaining circuit balance in this way expands the range over which ^{19}F resonance can be tuned without losing its match to 50 Ω.

The absence of a large conservative electric field in the low-E resonators greatly reduces the tuning and matching range needed to accommodate samples of varying hydration and salinity. This property plays very well into using low-voltage trimmers to reliably handle high levels of RF power. The resonance frequency and matching of the probe change very little upon sample insertion, so it is never necessary to adjust the piston positions of the trimmer capacitors to produce such a low capacitance that the voltage across the trimmer would increase beyond its ability to withstand. A properly chosen network of fixed capacitors can therefore serve as a voltage divider to protect the probe's vulnerable trimmer capacitors from arcing over a wide range of sample conditions. The capacitance of each trimmer can be estimated by counting the number of turns from the on-resonance position to the nearest piston stop. For the ^{1}H circuit, voltage dividers C_{4A} and C_{4B} were adjusted until the ratios of $(C_1 + C_2)/C_{4A}$ and C_3/C_{4B} were slightly larger than 1 in order to reduce the voltage across C_2 and C_3 by approximately 50%. The equivalent ratios $(C_7 + C_{7A})/C_{9A}$ and $(C_5 + C_6 + C_{6A})/C_{9B}$ for the ^{19}F network were set close to 2, reducing the voltages across the ^{19}F trimmers even further. Adjusting the balance for the outer ^{1}H resonator was accomplished by touching its top plane with the grounded wire and adjusting C_2 as reported previously [15]. The same could not be done for the ^{19}F resonator, since it is hidden within the ^{1}H resonator, so we measured the on-resonance piston position of the C_5 trimmer and modified chip values to satisfy $(C_{7A} - C_{6A}) \approx C_5$.

The orthogonal placement of the two resonators in the low-E assembly provides good intrinsic isolation between the ^{1}H and ^{19}F channels, despite only 6% difference in their Larmor frequencies. Small low-voltage parallel traps L_2–C_{10} and L_3–C_{11} were placed at the ^{1}H and ^{19}F ports, tuned to 564 and 600 MHz, respectively. For the circuit shown in Fig. 4, isolation between the ^{19}F and ^{1}H ports is 30 dB at the ^{1}H frequency and 23 dB at the ^{19}F frequency. Inductors L_2 and L_3 were made with just 1/2-turn of 2 mm wide flat wire (~10 nH), as can be seen in Fig. 3.

2.3. Reducing ^{19}F background from probe components

Eliminating the ^{19}F background signal requires careful selection of structural materials and RF circuit components. While rare in biological systems, fluorine is present in a wide range of commercial plastic materials. Fluoropolymers are particularly common in electronic components for radio and microwave circuits where they provide low dielectric loss at high frequencies and their high dielectric strength makes them an ideal choice for high voltage components. As originally constructed, our ^{19}F–^{1}H probe had produced a large ^{19}F background as shown in Fig. 5a. In subsequent tests we have found that fluorine-containing material must be removed not only from the proximity of the sample coil, but also from a distance below the coil that is determined by homogeneous volume of the magnet and by the width of the spectral window. The RF magnetic field produced by currents within coaxial cables and trimmer capacitors will interact with PTFE dielectrics and contribute ^{19}F background signal if static field B_0 at that location remains within the spectral window of the spectrometer. Complete elimination of background signal is therefore particularly difficult for wide bore magnet spectrometers, where B_0 homogeneity is maintained over a physically large volume. In our 600 MHz wide bore NMR spectrometer, achieving a background-free spectral window of 1 MHz (no detectable ^{19}F NMR signal after 10^4 scans) would require moving PTFE-containing trimmer capacitors and RF cables at least 13 cm away from the sample coil. Because doing so would present additional challenges for the high frequency matching networks, we

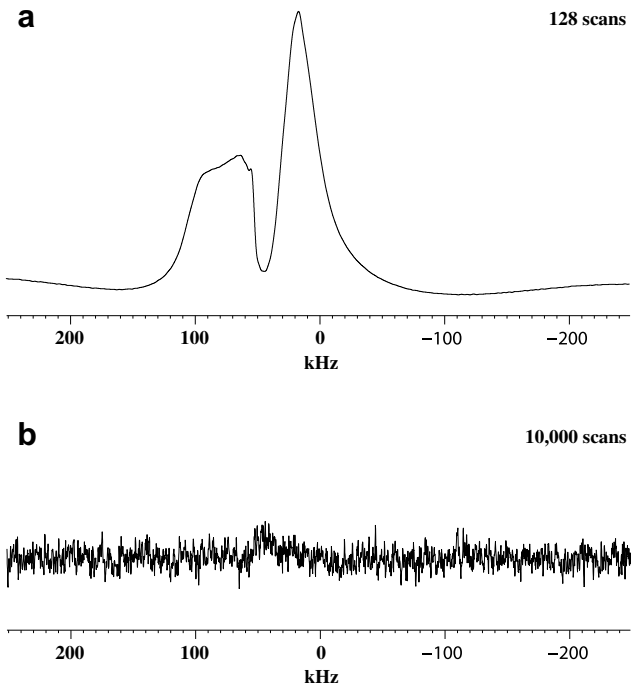

Fig. 5. Reduction of ^{19}F background signal in a single-pulse experiment (83 kHz ^{19}F B_1). Initially, a strong ^{19}F background signal ((a), 128 scans) was contributed by the coaxial cables and by the lubricant in the quartz trimmer capacitors. Removing the fluorinated material from these components (see Section 2.3) reduced the background NMR signal down to the noise level even after averaging as many as 10^4 transients (b).

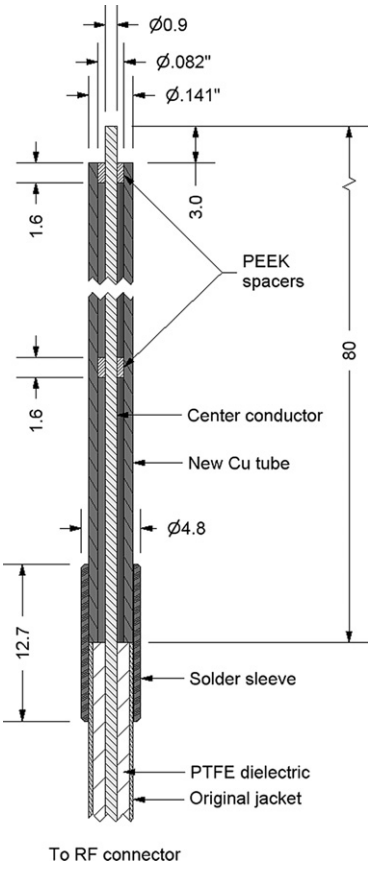

Fig. 6. Modified semi-rigid coaxial cable to reduce ^{19}F background signal from the PTFE dielectric. Dimensions are in millimeters unless noted otherwise.

chose to focus instead on modifying the RF components by stripping them of fluorine containing material.

Using trimmer capacitors with quartz or glass dielectric instead of PTFE is an obvious step but it still does not guarantee a fluorine-free probe. For example, the non-magnetic trimmer capacitors sold by Voltronics Corp. are now made with popular lubricants containing Teflon micro-particles, resulting in a strong ^{19}F background signal. We tested several in-house lubricants to find those that do not produce ^{19}F signal. We then ordered custom versions of the quartz trimmers with Dow-Corning silicone high-vacuum grease replacing the standard fluorinated lubricant for the piston screw. The Voltronics part numbers for these modified trimmers are V2687 (replaces NMQM3G) and V2688 (replaces NMQM6GENL). The capacitors made with vacuum grease produced no detectable ^{19}F signal.

Even more significant background signal came from the PTFE dielectric in the semi-rigid coaxial RF cables (.141″ OD, p/n, UT-141-C by MicroCoax Pottstown, PA) leading to the probe's ^{19}F and ^{1}H matching networks. Like the capacitors, these cables had to be modified by expunging the Teflon material, as shown in Fig. 6. The copper jacket and the PTFE dielectric were removed from the top 8 cm of each coaxial cable, exposing the bare center conductor. A custom copper tube was slid over the exposed region and then soldered to the original jacket with the help of a sleeve coupling. The copper tube was centered on the wire conductor by a few very short PolyEtherEther-Ketone (PEEK) spacers. To minimize reflection at the juncture, the inner diameter of the tube D was chosen to give a characteristic impedance of 50 Ω to match the original PTFE transmission line. This diameter was determined by using the formula:

$$Z_0 = \frac{138}{\sqrt{\varepsilon}} \log_{10} \frac{D}{d} = 50\ \Omega,$$

where d is the diameter of the center conductor and $\varepsilon = 1$ is the relative dielectric constant of air.

The variable temperature sample chamber around the coil was constructed of unfilled PEEK (Fig. 3). Other plastics used in the probehead were unfilled Ultem, and G-10/FR4 glass-filled resin rods for tuning trimmer capacitors. The trimmer capacitors were mounted below the VT chamber on a plate made of solid copper.

Fig. 5 shows the effect of removing fluorinated material from the trimmer capacitors and coaxial RF cables on the probe's ^{19}F background. Initially, while using commercial quartz trimmers and semi-rigid cables, a strong ^{19}F background signal had been observed in the empty probe after just 128 averages (Fig. 5a). After switching to fluorine-free

lubricant in the trimmer capacitors and removing PTFE in the RF cables (Fig. 6), the experiment was repeated with a spectral width of 1 MHz and 10^4 averages. The only remaining signal was a small bump at −45 kHz. Fig. 5b shows the central 500 kHz for comparison with the unmodified probe. A dead time of 50 μs was used for both plots. The shape, position, and intensity of the residual peak in Fig. 5b changes with the type of chip capacitors used in the RF circuit and seems to be connected to other small signals outside of the chemical shift range of ^{19}F. Therefore, we think that it is unlikely to be an NMR signal.

2.4. Measuring sample heat deposition

Measurements of RF-induced sample heating in the new ^{19}F–^{1}H probe were done using a technique described in our previous article [15]. Power efficiencies η of each channel were obtained by measuring the 360° pulse length and the power input at the base of the probe in the presence of lossy and non-lossy samples. The amount of heat q_{heat} deposited in the sample was then calculated in units of W/kHz^2 as

$$q_{\text{heat}} = \frac{1}{\eta_{\text{bio}}} - \frac{1}{\eta_{\text{nl}}}$$

where η_{bio} and η_{nl} are probe power efficiencies $\eta = (\omega_1/2\pi)^2/(AP_{\text{in}})$ in the presence and absence of sample loss, respectively. This formula is identical to one in [15], with exception of the minor correction coefficient $A < 1$ reflecting the fact that input power P_{in} is measured at the base of the probe. The actual power reaching matching network at the end of the probe's 50 Ω semi-rigid cable is AP_{in}. Both reference samples are made with a solution of equal parts 99.9% D_2O and trifluorethanol (TFE) to allow simultaneous 360° pulse measurement in the ^{19}F and ^{1}H channels. The lossy sample reference also contained 100 mM of NaCl in order to raise the ionic conductivity. The D_2O/TFE solution was sealed inside the standard rectangular glass cell (New Era Enterprises, Vineland, NJ, p/n SK-190505-1) with each sample occupying the precise rectangular sample space of $6 \times 4 \times 9$ mm. Our goal for this probe was to reduce ^{19}F and ^{1}H sample heating in ^{19}FCPMG experiments to the level achieved by the PISEMA probe reported in our previous article. To establish a basis for comparison, q_{heat} for the same set of D_2O/TFE samples was also measured in the 600 MHz low-E PISEMA probe previously described in [15] as low-E coil II.

3. Results

Pulse lengths for the D_2O/TFE samples with and without 100 mM NaCl were first measured in the 600 MHz low-E PISEMA probe. When analyzed as described in above paragraph, it was determined that ^{1}H power absorption by the lossy sample in that probe was 6.3 ± 0.5 mW/kHz^2. The measurements were then repeated for both channels of the new low-E fluorine probe. In the new probe, the amount of power q_{heat} absorbed by the 100 mM D_20/TFE sample was actually reduced to 3.8 ± 0.3 and 3.6 ± 0.3 mW/kHz^2 for the ^{19}F and ^{1}H channels, respectively. Smaller sample heating in the ^{1}H channel of fluorine probe is probably due to the partial shielding of ^{1}H electric field by the top and bottom conductive planes of the inner ^{19}F resonator. The degree of tuning shift upon insertion of different samples is also important experimentally, as described above, and depends on the level of electric field in the sample. Insertion of the 100 mM sample into the empty probe resulted in tuning shifts of only 0.13 MHz for the ^{19}F resonance and 0.95 MHz for the ^{1}H resonance, indicating that only a fairly small electric field was present in the sample. The RF field homogeneity over the $6 \times 4 \times 9$ mm sample volume was measured as the ratio of 810° to 90° pulse amplitudes for both ^{19}F and ^{1}H channels. The ratios were found to be 83% in the ^{19}F and 93% in the ^{1}H channels. It is worth pointing out that the length of the test sample was nearly the same as that of the ^{19}F resonator. RF fields $\omega_1/2\pi = 100$ kHz were achieved for the non-lossy sample at 330 W of input power in the ^{19}F channel and at 695 W in the ^{1}H channel. The power efficiency of the ^{1}H channel is notably smaller than that of the low-E PISEMA probe, which achieved 100 kHz at 380 W. We attribute the loss to the non-zero z-axis component of the ^{1}H B_1 field near the top and bottom planes of the ^{19}F resonator (Fig. 1). It may induce ^{1}H eddy currents in these horizontal planes that are not removed by slotting the ^{19}F resonator. However, since the ^{1}H channel in this probe is used solely for decoupling and not for detection, the reduced ^{1}H efficiency does not affect the NMR experiment. It means only that we need to have an amplifier with sufficient power to produce the desired B_1. Intuitively, one might erroneously conclude that having to apply more decoupling power will lead to more sample heating. In fact, RF loss in the sample is a function of electric-to-magnetic field ratio E/ω_1 which depends on coil geometry and not on power efficiency [14]. Isolation between the ^{19}F and ^{1}H ports provided within the probe was measured 30 dB at the ^{1}H frequency and 23 dB at the ^{19}F frequency. Further isolation of at least 80 dB can be achieved by additional external filters.

The experimental capabilities of the ^{19}F–^{1}H low-E probe are demonstrated in Fig. 7. It shows both experimental (Fig. 7a) and simulated (Fig. 7b) two-dimensional^{19}FCPMG spectra of Flufenamic acid (FFA), a non-steroidal anti-inflammatory drug, aligned in hydrated DMPC lipid bilayers. The experiment was conducted using a Bruker DRX 600 NMR wide bore spectrometer (14.1 Tesla) at the National High Magnetic Field Laboratory. The CPMG experiment was performed in two dimensions to correlate dipolar coupling with the chemical shift, as in PISEMA experiments. The CPMG multi-pulse sequence [17,18] was used in the indirect, t_1, dimension to suppress all interactions except for ^{19}F homonuclear dipolar couplings, resulting in pure dipolar spectra of spin pairs, while the ^{19}F anisotropic chemical shift and dipolar coupling were observed in the t_2 dimension. An XY-4 phase cycling

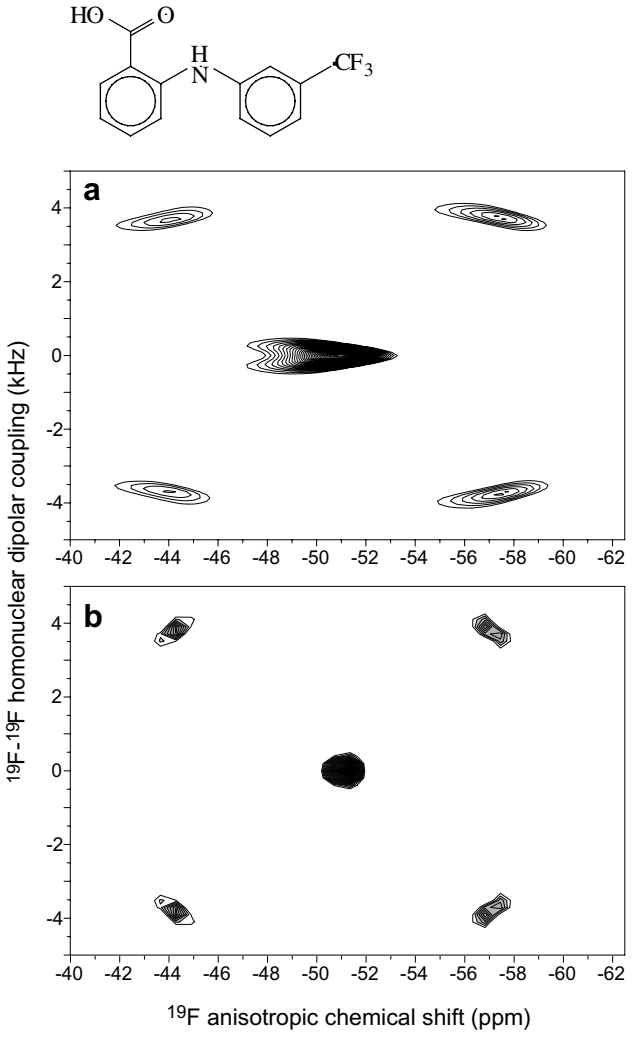

Fig. 7. Experimentally obtained (a) and simulated (b) two-dimensional ^{19}FCPMG spectra of Flufenamic acid (see top diagram) aligned in DMPC bilayers (1:16 molar ratio, fully hydrated, at 35 °C). In this experiment (a), the echo time of 10 μs was used and for each t_1 increment. Four 180° pulses were used with an XY-4 phase cycling scheme [25] to minimize the 180° pulse imperfections, giving rise to an effective dwell time of 18.75 μs in the t_1 dimension. With 256 t_1 increments, 64 transients, and 1 s recycle time, acquisition time was 34 min. ^{19}F $B_1 = 100$ kHz, ^{1}H B_1 (decoupling) = 70 kHz. Simulation in (b) was done using Simpson software [27] with above NMR parameters, CSA powder pattern ≈ 12 ppm and order parameter $S_{CF3} \approx 0.18$ [26].

scheme [25] was employed in the t_1 dimension to minimize the 180° pulse imperfections. Experimental parameters are described in the caption to Fig. 7. The center peak at −51.0 ppm in Fig. 7a represents the anisotropic chemical shift of the CF_3 of the FFA aligned in the lipid bilayers. Its isotropic chemical shift is −62 ppm. The outer two peaks in the ω_2 dimension, 3.8 kHz away from the center peak, stem from the homonuclear dipolar coupling in the CF_3 group. This homonuclear dipolar coupling is verified in the ω_1 dimension of the 2D CPMG spectrum (Fig. 7a) where two intense peaks appear at around ±3.8 kHz, which is close to the previous measurements [26]. Fig. 7b shows simulation of the same FFA compound using the SIMPSON software package [27], with the same NMR parameters as in Fig. 7 caption and with CSA powder pattern ≈12 ppm and order parameter $S_{CF3} \approx 0.18$ [26]. All main features of the simulation match well the experimental spectrum. Interestingly, it can be noticed from Fig. 7a that the ^{19}F anisotropic chemical shift spans a range of ~3 ppm while the ^{19}F dipolar coupling appears to be dependent on the ^{19}F anisotropic chemical shift position, which cannot be seen in 1D experiments. This may imply that the time-averaged director of such an aligned molecule wobbles at a small degree around the axis parallel to the bilayer normal.

4. Conclusion and discussion

The design and application of a large volume and sample-friendly solid state NMR probe has been demonstrated for ^{19}F CPMG studies in hydrated and lossy oriented protein preparations at 600 MHz. We built upon a previously reported ^{15}N–^{1}H low-E probe design [15], where use of a separate loop-gap resonator reduced ^{1}H decoupler heating by an order of magnitude compared to a conventional solenoid. Replacing the ^{15}N observe solenoid with another loop-gap resonator for the ^{19}F channel produced a probe that minimizes conservative electric fields, and their corresponding sample loss, in both ^{19}F and ^{1}H channels. This has benefits to ^{19}FCPMG and related multi-pulse experiments, in which the sample is subjected to RF irradiation with high duty cycles at both ^{19}F and ^{1}H frequencies. Without the strong conservative electric field of a solenoid, the probe's tuning and matching need only a small adjustment upon insertion of hydrated and salty samples. In each of the new probe's two channels, dissipation of RF power within a lossy biological sample is smaller than in the decoupling channel of the low-E ^{15}N–^{1}H probe. The loop-gap resonators provide excellent RF homogeneity across the sample in each channel, benefiting cross-polarization efficiency. Absence of wavelength effects in the loop-gap resonators enables the study of large sample volumes at high fields. The orthogonal placement of independent ^{19}F and ^{1}H resonators greatly simplified the issue of channel separation, allowing ⩾23 dB of isolation within the probe itself and ⩾80 dB with external inline filters. It also resulted in convenient tuning, where adjustment of either resonance does not affect the other one. Finally, the elimination of fluorinated materials from the probe, which involved modification of trimmer capacitors and construction of custom 50 Ω coaxial cables, resulted in a 1 MHz-wide spectral window free of ^{19}F background NMR signal after 10^4 averages. The low-E ^{19}F–^{1}H probehead design described in this paper need not be limited to the static applications and could be implemented in MAS stators in a manner similar to that discussed in [28].

Acknowledgments

This work was supported by NSF Cooperative agreement (DMR 00884173), the State of Florida, and by In-House Research Program at the National High Magnetic

Field Laboratory. We thank Prof. Timothy A. Cross for encouragement and for support. R.W. acknowledges support from Forschungszentrum Karlsruhe and DFG-CFN from University of Karlsruhe. E.Y.C's. position was supported by NIH PO1-GM-64676 to T.A. Cross. We also wish to acknowledge Richard Desilets for fabrication of the parts used in the probe.

References

[1] S.L. Grage, J.F. Wang, T.A. Cross, A.S. Ulrich, Solid-state F-19-NMR analysis of F-19-labeled tryptophan in gramicidin A in oriented membranes, Biophys. J. 83 (2002) 3336–3350.

[2] A.S. Ulrich et al., Solid-state 19F NMR analysis of membrane-active peptides, in: A. Ramamoorthy (Ed.), NMR Spectroscopy of Biological Solids, Taylor & Francis, 2004, p. 215.

[3] A.S. Ulrich, Solid state F-19 NMR methods for studying biomembranes, Prog. Nucl. Magn. Reson. Spectrosc. 46 (2005) 1–21.

[4] W.E. Hull, B.D. Sykes, Fluorotyrosine alkaline-phosphotase—internal mobility of individual tyrosines and role of chemical shift anisotropy as a F-19 nuclear spin relaxation mechanism in proteins, J. Mol. Biol. 98 (1975) 121–153.

[5] A.C. de Dios, J.G. Pearson, E. Oldfield, Secondary and tertiary structural effects on protein NMR chemical shifts: an ab initio approach, Science 260 (1993) 1491–1496.

[6] D. O'Hagan, D.B. Harper, Fluorine containing natural products, J. Fluoresc. Chem. 100 (1999) 127–133.

[7] J.G. Pearson et al., Chemical-shifts in proteins - a shielding trajectory analysis of the fluorine nuclear-magnetic-resonance spectrum of the *Escherichia coli* galactose binding-protein using a multipole shielding polarizability local reaction field molecular-dynamics approach, J. Am. Chem. Soc. 115 (1993) 6851–6862.

[8] R.W. Martin, E.K. Paulson, K.W. Zilm, Design of a triple resonance magic angle sample spinning probe for high field solid state nuclear magnetic resonance, Rev. Sci. Instrum. 74 (2003) 3045–3061.

[9] S.V. Dvinskikh, V. Castro, D. Sandström, Heating caused by radiofrequency irradiation and sample rotation in ^{13}C magic angle spinning NMR studies of lipid membranes, Magn. Reson. Chem. 42 (2004) 875–881.

[10] C. Li, Y. Mo, J. Hu, E.Y. Chekmenev, C. Tian, F.P. Gao, R. Fu, P.L. Gor'kov, W.W. Brey, T.A. Cross, Analysis of RF heating and sample stability in aligned static solid state NMR spectroscopy, J. Magn. Reson. 180 (2006) 51–57.

[11] D.I. Hoult, P.C. Lauterbur, Sensitivity of the zeugmatographic experiment involving human samples, J. Magn. Reson. 34 (1979) 425–433.

[12] J.B.D. de Lacaillerie, B. Jarry, O. Pascui, D. Reichert, "Cooking the sample": Radiofrequency induced heating during solid-state NMR experiments, Sol. State Nuc. Magn. Reson. 28 (2005) 225–232.

[13] J.A. Stringer, C.E. Bronnimann, C.G. Mullen, D.H. Zhou, S.A. Stellfox, Y. Li, E.H. Williams, C.M. Rienstra, Reduction of RF-induced sample heating with a scroll coil resonator structure for solid-state NMR probes, J. Magn. Reson. 173 (1) (2005) 40–48.

[14] F.D. Doty, J. Kulkarni, C. Turner, G. Entzminger, A. Bielecki, Using a cross-coil to reduce RF heating by an order of magnitude in triple-resonance multinuclear MAS at high fields, J. Magn. Reson. 182 (2) (2006) 239–253.

[15] P.L. Gor'kov, E.Y. Chekmenev, C. Li, M. Cotten, J.J. Buffy, N.J. Traaseth, G. Veglia, W.W. Brey, Using low-E resonators to reduce RF heating in biological samples for static solid-state NMR up to 900 MHz, J. Magn. Reson. 185 (2007) 77–93.

[16] B. Dillmann, K. Elbayed, H. Zeiger, M.-C. Weingertner, M. Piotto, F. Engelke, A novel low-E field coil to minimize heating of biological samples in solid-state multinuclear NMR experiments, J. Magn. Reson. 187 (2007) 10–18.

[17] H.Y. Carr, E.M. Purcell, Effects of diffusion on free precession in nuclear magnetic resonance experiments, Phys. Rev. 94 (1950) 630–638.

[18] S. Meiboom, D. Gill, Modified spin-echo method for measuring nuclear relaxation times, Rev. Sci. Instrum. 29 (1958) 688–691.

[19] J.R. Fitzsimmons, H.R. Brooker, B. Beck, A comparison of double-tuned surface coils, Magn. Reson. Med. 10 (1989) 302–309.

[20] S. Kan, P. Gonord, Single-input double-tuned mutually coupled surface coil circuits—an analysis, Rev. Sci. Instrum. 62 (1991) 2427–2429.

[21] S.L. Hu, J.A. Reimer, A.T. Bell, Single-input double-tuned circuit for double resonance nuclear magnetic resonance experiments, Rev. Sci. Instrum. 69 (1998) 477–478.

[22] J. Haase, N.J. Curro, C.P. Slichter, Double resonance probes for close frequencies, J. Magn. Reson. 135 (1998) 273–279.

[23] S.P. Graether, J.S. DeVries, R. McDonald, M.L. Rakovszky, B.D. Sykes, A $^{1}H/^{19}F$ minicoil NMR probe for solid-state NMR: Application to 5-fluoroindoles, J. Magn. Reson. 178 (2006) 65–71.

[24] D.W. Alderman, D.M. Grant, Efficient decoupler coil design which reduces heating in conductive samples in superconducting spectrometers, J. Magn. Reson. 36 (1979) 447–451.

[25] A.A. Maudsley, Modified Carr–Purcell–Meiboom–Gill sequence for NMR Fourier-imaging applications, J. Magn. Reson. 69 (1986) 488–491.

[26] S.L. Grage, A.S. Ulrich, Orientation-dependent F-19 dipolar couplings within a trifluoromethyl group are revealed by static multipulse NMR in the solid state, J. Magn. Reson. 146 (2000) 81–88.

[27] M. Bak, J.T. Rasmussen, N.C. Nielsen, SIMPSON: a general simulation program for solid-state NMR spectroscopy, J. Magn. Reson. 147 (2000) 296–330.

[28] S.A. McNeill, P.L. Gor'kov, J. Struppe, W.W. Brey, J.R. Long, Optimizing ssNMR for dilute proteins in heterogeneous mixtures at high magnetic fields, Magn. Reson. Chem. (2007), in press.